UNIVERSITY OF AMSTERDAM

Master Astronomy and Astrophysics - 5214RAAS6Y

Radio Astronomy

Lecture 9

Time-Domain I: Single-dish techniques

Lecturer: Joeri van Leeuwen (leeuwen@astron.nl)

May 6th 2013

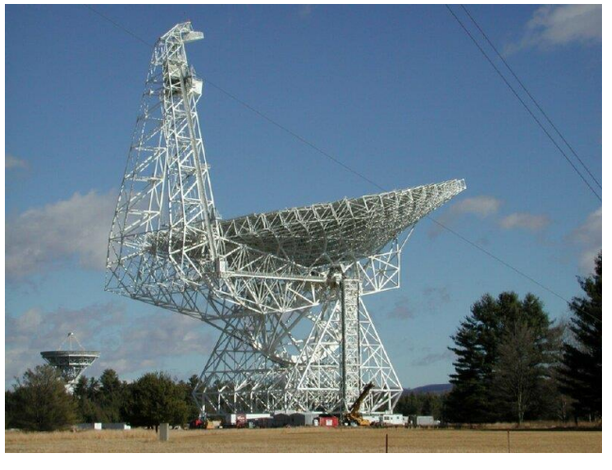

Lecture Outline

- 1st hour:
  Imaging vs. single-dish / time-domain
  High-time resolution recording
  Pulsar properties

- 2nd hour:
  Pulsar properties continued
  Pulsar timing

Imaging vs. time-domain

- Imaging:
  Synthesis; correlation; time-integration

- Time-domain:
  Single dish (“photon bucket”)
  Beam-forming (more next week)
  Fast sampling
  Usually: one “pixel”

Online data sampling

Square-law detectors are not used these days. The receiver produces a varying analogue output voltage that is usually digitised and stored for further (offline) processing.

How often must we sample the signal ?

Consider the following sine wave:

If we sample once per cycle time (period) we would consider the signal to have a constant amplitude.

If we sample twice per cycle time (period) we get a saw-tooth wave that is becoming a good approximation to a sinusoid.

For lossless digitisation we must sample the signal at least twice per cycle time.

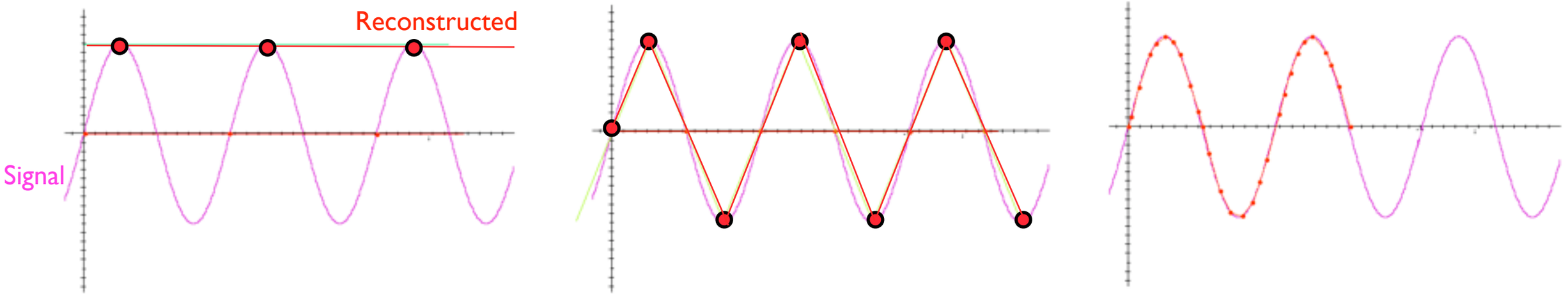

Nyquist's sampling theorem states that for a limited bandwidth signal with maximum frequency f_{max}, the equally spaced sampling frequency f_s must be greater than twice the maximum frequency f_{max}, i.e. $f_s > 2\ f_{max}$ in order for the signal to be uniquely reconstructed without aliasing.

The frequency $2f_{max}$ is called the Nyquist sampling rate.

e.g. If a reciever system provides a baseband signal of 20 MHz, the signal must be sampled 40E6 times per second.

Note that strictly speaking, the sampling frequency (rate) must be strictly greater than the Nyquist rate ($f_s > 2 \cdot f_{max}$) of the signal to achieve unambiguous representation of the signal. In the pathlogical case where the signal contains a frequency component at precisely the Nyquist frequency, then the corresponding component of the sample values cannot have sufficient information to reconstruct the signal.

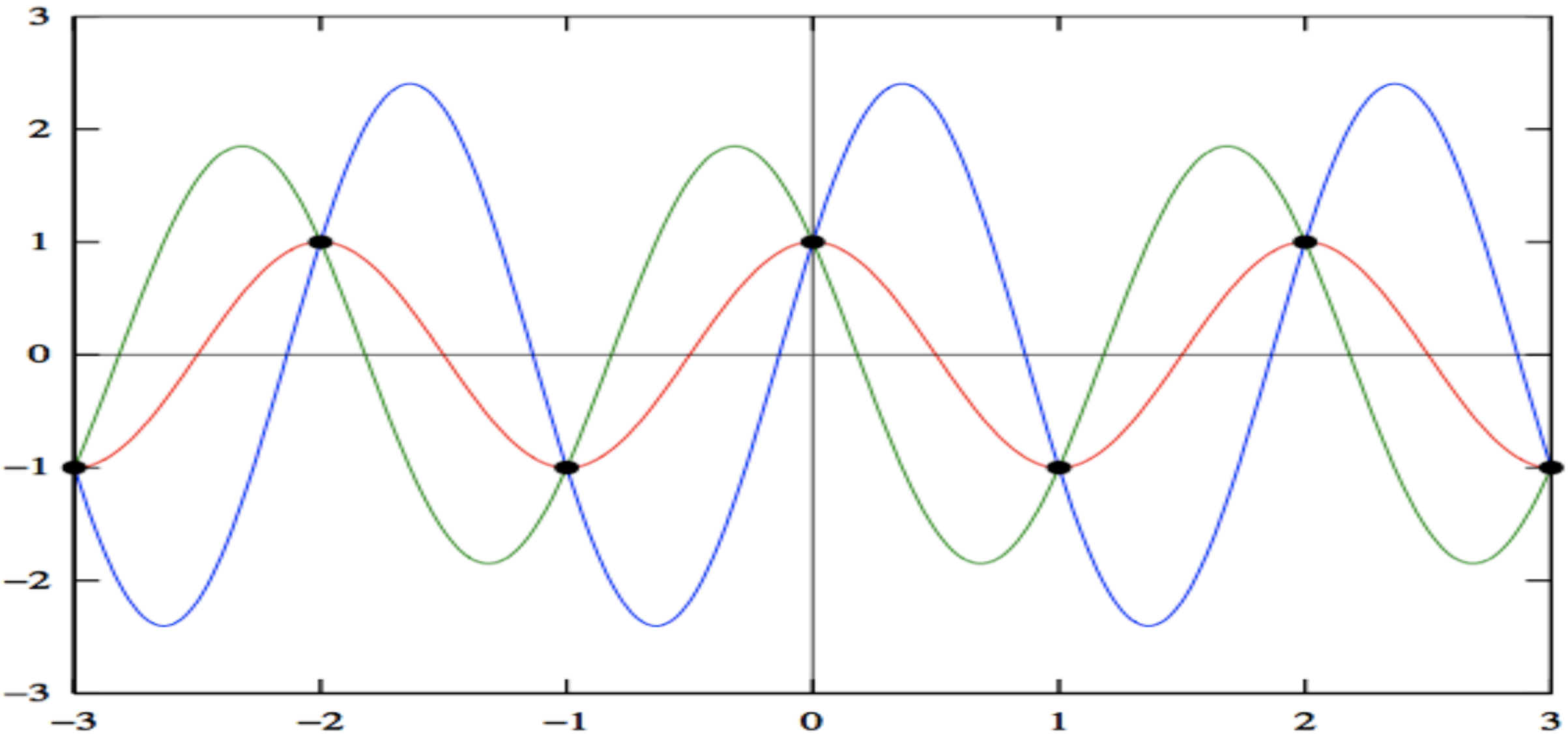

A family of sinusoids at the critical frequency, all having the same sample sequences of alternating +1 and −1. That is, they all are aliases of each other, even though their frequency is not above half the sample rate. Note that strictly speaking, the sampling frequency (rate) must be strictly greater than the Nyquist.

Sampling at less than the Nyquist rate leads to aliasing of the original signal (right).

Since the final processing of radio astronomy data takes place via digital computers, devices known as *Analogue to digital converters* (ADC) are used to sampled at regular intervals the voltage signal from the receiver.

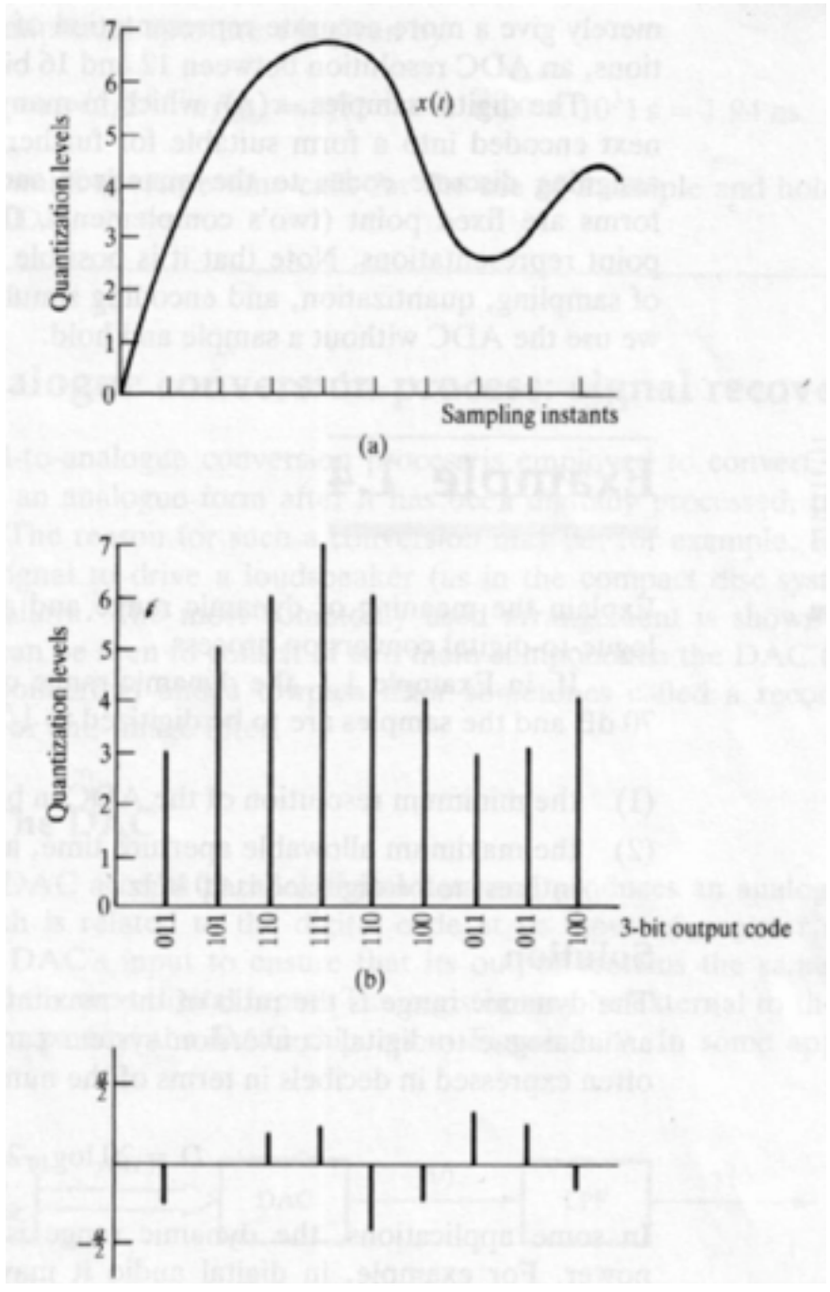

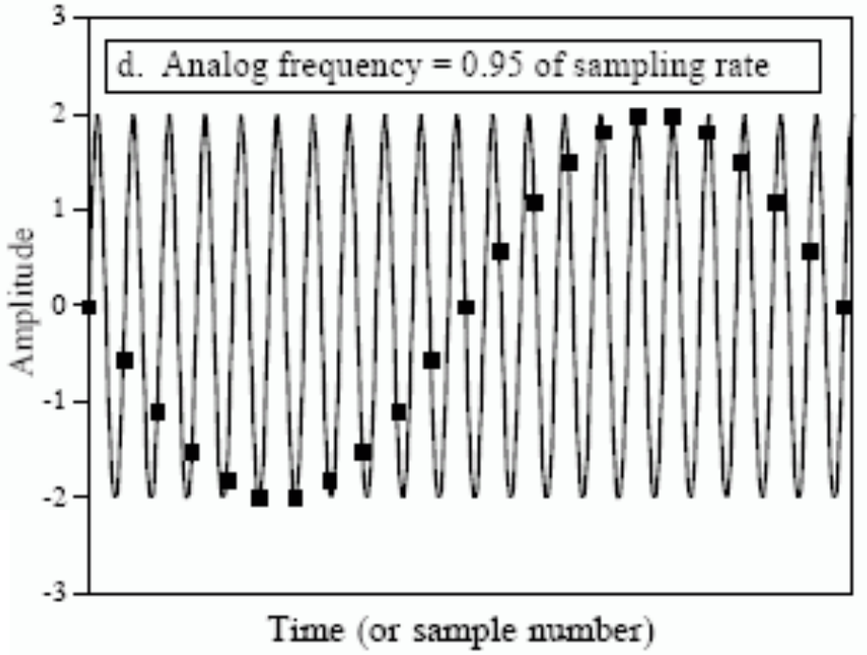

The sampling frequency employed is usually the Nyquist rate or sometimes the signal may be over-sampled.

The number of bits (referred to as the quantisation) used for one value of the discrete signal sets the accuracy of the signal magnitude.

Left: a 3-bit (9 level) quantisation is used [b] in order to characterise the original signal [a]. The errors (or residuals) are shown in [c].

Somewhat surprisingly, even low levels of quantisation result in a relatively modest degredation in signal-to-noise, at least in the case where the signals are not strong:

No. of Bits	Relative performance
1	64%
2	81%
3	88%
infinity	100%

2-bit samples are commonly used in current radio telescope systems. As can be seen from the table, the degredation of the signal-to-noise for 2-bit sampling is much less than that of 1-bit sampling, the value achieved is 0.88 of an ideal system. A larger number of bits can be used but the point of diminishing returns is rapidly reached and the compute burden begins to rise with for very little real gain.

The table (left) assumes Nyquist sampling. Some modest gains can be made by also increasing the sample rate.

This analysis is correct assuming we are sampling signals with a limited range of power. The process of quantisation is inherintely non-linear, and in the presence of strong signals (such as RFI) a larger number of bits is required to characterise the wide range of signal strength.

e.g. LOFAR uses 12-bit samples... leading to very large data rates!

e.g. LOFAR operates with a bandwidth of 48 MHz. With Nyquist sampling, each LOFAR station generates 48E6 x 2 x 12 bits ~ 1.1 Gbit per second per polarisation product.

Pulsar Properties

Known radio pulsars appear to emit short pulses of radio radiation with pulse periods between 1.4 ms and 8.5 seconds. Even though the word ***pulsar*** is a combination of "pulse" and "star," pulsars are not pulsating stars. Their radio emission is actually continuous but beamed, so any one observer sees a pulse of radiation each time the beam sweeps across his line-of-sight. Since the pulse periods equal the rotation periods of spinning neutron stars, they are quite stable. Even though the radio emission mechanism is not well understood, radio observations of pulsars have yielded a number of important results because:

(1) Neutron stars are physics laboratories providing extreme conditions (deep gravitational potentials, densities exceeding nuclear densities, magnetic field strengths as high as $B \sim 10^{14}$ or even 10^{15} gauss) not available on Earth.

(2) Pulse periods can be measured with accuracies approaching 1 part in 10^{16}, permitting exquisitely sensitive measurements of small quantities such as the power of gravitational radiation emitted by a binary pulsar system or the gravitational perturbations from planetary-mass objects orbiting a pulsar.

The radical proposal that neutron stars exist was made with trepidation by Baade & Zwicky in 1934: "*With all reserve we advance the view that a supernova represents the transition of an ordinary star into a new form of star, the* ***neutron star****, which would be the end point of stellar evolution. Such a star may possess a very small radius and an extremely high density.*" Pulsars provided the first evidence that neutron stars really do exist. They tell us about the strong nuclear force and the nuclear equation of state in new ranges of pressure and density, test general relativity and alternative theories of gravitation in both shallow and relativisitically deep ($GM/(rc^2) \gg 0$) potentials, and led to the discovery of the first extrasolar planets.

Discovery and Basic Properties

Pulsars were discovered serendipidously in 1967 on chart-recorder records obtained during a low-frequency ($\nu = 81$ MHz) survey of extragalactic radio sources that scintillate in the interplanetary plasma, just as stars twinkle in the Earth's atmosphere. This important discovery remains a warning against overprocessing data before looking at them, ignoring unexpected signals, and failing to explore observational "parameter space" (here the relevant parameter being time). As radio instrumentation and data-taking computer programs become more sophisticated, signals are "cleaned up" before they reach the astronomer and optimal "matched filtering" tends to suppress the unexpected. Thus clipping circuits are used to remove the strong impulses that are usually caused by terrestrial interference, and integrators smooth out fluctuations shorter than the integration time. Pulsar signals "had been recorded but not recognized" several years earlier with the 250-foot Jodrell Bank telescope. Most pulses seen by radio astronomers are just artificial interference from radar, electric cattle fences, etc., and short pulses from sources at astronomical distances imply unexpectedly high brightness temperatures $T_\mathrm{b} \sim 10^{25}$–$10^{30}$ K $\gg 10^{12}$ K, the upper limit for incoherent electron-synchrotron radiation set by inverse-Compton scattering.

However, Cambridge University graduate student Jocelyn Bell noticed pulsars in her scintillation survey data because the pulses appeared earlier by about 4 minutes every solar day, so they appeared exactly once per sidereal day and thus came from outside the solar system.

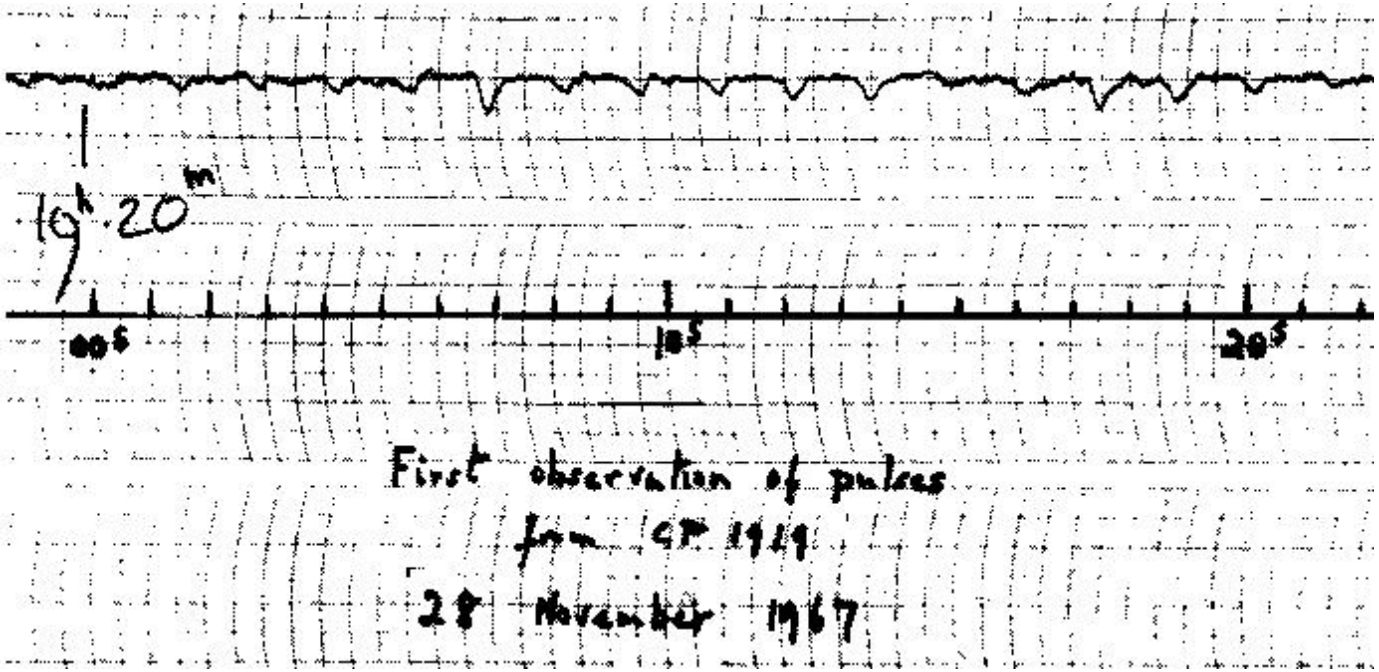

Figure 1. "High-speed" chart recording of the first known pulsar, CP1919. This confirmation observation showed that the "scruffy" signals observed previously were periodic.

The sources and emission mechanism were originally unknown, and even intelligent transmissions by LGM ("little green men") were seriously suggested as explanations for pulsars. Astronomers were used to slowly varying or pulsating emission from stars, but the natural period of a radially pulsating star depends on its mean density ρ and is typically days, not seconds. Likewise there is a lower limit to the rotation period P of a gravitationally bound star, set by the requirement that the centrifugal acceleration at its equator not exceed the gravitational acceleration. If a star of mass M and radius R rotates with angular velocity $\Omega = 2\pi/P$,

$$\Omega^2 R < \frac{GM}{R^2}$$

$$\frac{4\pi^2 R^3}{P^2} < GM$$

$$P^2 > \left(\frac{4\pi R^3}{3}\right)\frac{3\pi}{GM}$$

In terms of the mean density

$$\rho = M\left(\frac{4\pi R^3}{3}\right)^{-1},$$

$$P > \left(\frac{3\pi}{G\rho}\right)^{1/2}$$

or

$$\boxed{\rho > \frac{3\pi}{GP^2}} \quad (6A1)$$

This is actually a very conservative lower limit to ρ because a rapidly spinning star becomes oblate, increasing the centrifugal acceleration and decreasing the gravitational acceleration at its equator.

Example: The first pulsar discovered (CP 1919+21, where the "CP" stands for *Cambridge pulsar*) has a period $P = 1.3$ s. What is its minimum mean density?

$$\rho > \frac{3\pi}{GP^2} = \frac{3\pi}{6.67 \times 10^{-8}\ \text{dyne cm}^2\ \text{gm}^{-2}(1.3\ \text{s})^2} \approx 10^8\ \text{g cm}^{-3}$$

This density limit is just consistent with the densities of white-dwarf stars. But soon the faster ($P = 0.033$ s) pulsar in the Crab Nebula was discovered, and its period implied a density too high for any stable white dwarf. The Crab nebula is the remnant of a known supernova recorded by ancient Chinese astronomers as a "guest star" in 1054 AD, so the discovery of this pulsar also confirmed the Baade & Zwicky suggestion that neutron stars are the compact remnants of supernovae. The fastest known pulsar (discovered by Jason!) has $P = 1.4 \times 10^{-3}$ s implying $\rho > 10^{14}$ g cm^{-3}, the density of nuclear matter. For a star of mass greater than the ***Chandrasekhar mass***

$$M_{\rm Ch} \approx \left(\frac{hc}{2\pi G}\right)^{3/2} \frac{1}{m_{\rm p}^2} \approx 1.4 M_\odot$$

(compact stars less massive than this are stable as white dwarfs), the maximum radius is

$$R < \left(\frac{3M}{4\pi\rho}\right)^{1/3}$$

In the case of the $P = 1.4 \times 10^{-3}$ pulsar with $\rho > 10^{14}$ g cm^{-3},

$$R < \left(\frac{3 \times 1.4 \times 2.0 \times 10^{33}\ \text{g}}{4\pi \times 10^{14}\ \text{g cm}^{-3}}\right)^{1/3} \approx 2 \times 10^6\ \text{cm} \approx 20\ \text{km}$$

The ***canonical neutron star*** has $M \approx 1.4 M_\odot$ and $R \approx 10$ km, depending on the equation-of-state of extremely dense matter composed of neutrons, quarks, etc. The extreme density and pressure turns most of the star into a neutron superfluid that is a superconductor up to temperatures $T \sim 10^9$ K. Any star of significantly higher mass ($M \sim 3 M_\odot$ in standard models) must collapse and become a black hole. The masses of several neutron stars have been measured with varying degrees of accuracy, and all turn out to be very close to $1.4 M_\odot$.

The Sun and many other stars are known to possess roughly dipolar magnetic fields. Stellar interiors are mostly ionized gas and hence good electrical conductors. Charged particles are constrained to move along magnetic field lines and, conversely, field lines are tied to the particle mass distribution. When the core of a star collapses from a size $\sim 10^{11}$ cm to $\sim 10^6$ cm, its magnetic flux $\Phi \equiv \int \vec{B} \cdot \vec{n}\, da$ is conserved and the initial magnetic field strength is multiplied by $\sim 10^{10}$, the factor by which the cross-sectional area a falls. An initial magnetic field strength of $B \sim 100$ G becomes $B \sim 10^{12}$ G after collapse, so young neutron stars should have very strong dipolar fields. The best models of the core-collapse process show that a dynamo effect may generate an even larger magnetic field. Such dynamos are thought to be able to produce the $10^{14} - 10^{15}$G fields in ***magnetars***, neutron stars having such strong magnetic fields that their radiation is powered by magnetic field decay. Conservation of angular momentum during collapse increases the rotation rate by about the same factor, 10^{10}, yielding initial periods in the millisecond range. Thus young neutron stars should drive rapidly rotating magnetic dipoles.

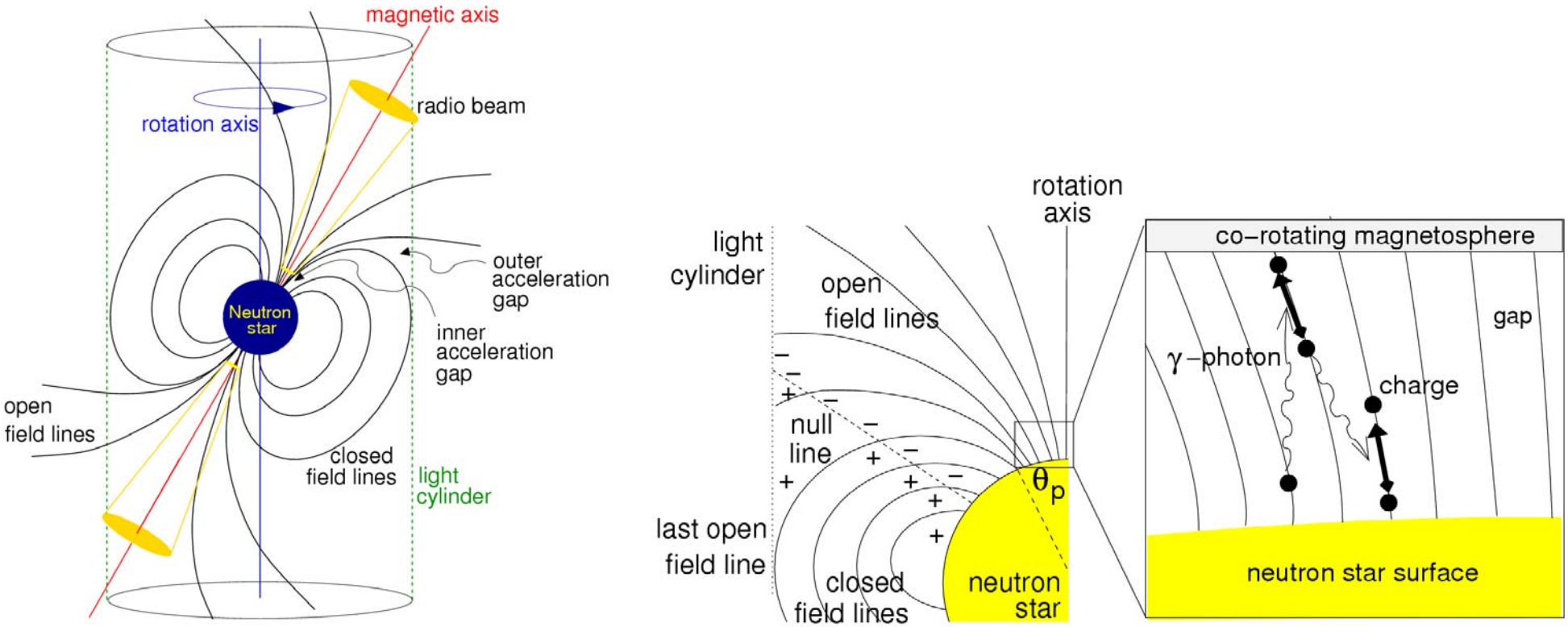

Figure 2: A Pulsar. (left): A diagram of the traditional magnetic dipole model of a pulsar. (right) Diagram of a simple dipole magnetic field near the polar caps. The inset figure shows a schematic of the electon-positron cascade which is required by many models of coherent pulsar radio emission (Both figures are from the Handbook of Pulsar Astronomy by Lorimer and Kramer).

Energetics

If the ***magnetic dipole*** is inclined by some angle $\alpha > 0$ from the rotation axis, it emits low-frequency electromagnetic radiation. Recall the Larmor formula for radiation from a rotating electric dipole:

$$P_{\rm rad} = \frac{2q^2\dot{v}^2}{3c^3} = \frac{2}{3}\frac{(q\ddot{r}\sin\alpha)^2}{c^3} = \frac{2}{3}\frac{(\ddot{p}_\perp)^2}{c^3} \ ,$$

where $p_\perp$ is the perpendicular component of the electric dipole moment. By analogy, the power of the ***magnetic dipole radiation*** from an inclined magnetic dipole is

$$\boxed{P_{\rm rad} = \frac{2}{3}\frac{(\ddot{m}_\perp)^2}{c^3}} \qquad (6A2)$$

where $m_\perp$ is the perpendicular component of the magnetic dipole moment. For a uniformly magnetized sphere with radius R and surface magnetic field strength B, the magnetic dipole moment is (see Jackson's *Classical Electrodynamics*)

$$m = BR^3 \ .$$

If the inclined magnetic dipole rotates with angular velocity Ω,

$$m = m_0 \exp(-i\Omega t)$$

$$\dot{m} = -i\Omega m_0 \exp(-i\Omega t)$$

$$\ddot{m} = \Omega^2 m_0 \exp(-i\Omega t) = \Omega^2 m$$

so

$$P_{\text{rad}} = \frac{2}{3}\frac{m_\perp^2 \Omega^4}{c^3} = \frac{2m_\perp^2}{3c^3}\left(\frac{2\pi}{P}\right)^4 = \frac{2}{3c^3}(BR^3 \sin\alpha)^2\left(\frac{2\pi}{P}\right)^4 ,$$

where P is the pulsar period. This electromagnetic radiation will appear at the *very* low frequency $\nu = P^{-1} < 1$ kHz, so low that it cannot be observed, or even propagate through the ionized ISM. The huge power radiated is responsible for pulsar slowdown as it extracts rotational kinetic energy from the neutron star. The absorbed radiation can also light up a surrounding nebula, the Crab nebula for example.

The rotational kinetic energy $E_{\rm rot}$ is related to the moment of inertia I by

$$E_{\rm rot} = \frac{1}{2} I \Omega^2 = \frac{2\pi^2 I}{P^2} \ .$$

Example: The moment of inertia of the "canonical" neutron star (uniform-density sphere with $M \approx 1.4 M_\odot$ and $R \approx 10$ km) is

$$I = \frac{2}{5} M R^2 \approx \frac{2 \cdot 1.4 \cdot 2.0 \times 10^{33} \ {\rm g} \cdot (10^6 \ {\rm cm})^2}{5} \approx 10^{45} \ {\rm gm \ cm^2}$$

Therefore the rotational energy of the Crab pulsar ($P = 0.033$ s) is

$$E_{\rm rot} = \frac{2\pi^2 I}{P^2} \approx \frac{2\pi^2 \cdot 10^{45} \ {\rm g \ cm^2}}{(0.033 \ {\rm s})^2} \approx 1.8 \times 10^{49} \ {\rm ergs}$$

Pulsars are observed to slow down gradually:

$$\dot{P} \equiv \frac{dP}{dt} > 0$$

Note that $\dot{P}$ is dimensionless (e.g., seconds per second). From the observed period P and period derivative $\dot{P}$ we can estimate the rate at which the rotational energy is decreasing.

$$\frac{dE_{\text{rot}}}{dt} = \frac{d}{dt}\left(\frac{1}{2}I\Omega^2\right) = I\Omega\dot{\Omega}$$

$$\Omega = \frac{2\pi}{P} \qquad \text{so} \qquad \dot{\Omega} = 2\pi(-P^{-2}\dot{P}), \quad \text{and}$$

$$\frac{dE_{\text{rot}}}{dt} = I\Omega\dot{\Omega} = I\frac{2\pi}{P}\frac{2\pi(-\dot{P})}{P^2}$$

$$\boxed{\frac{dE_{\text{rot}}}{dt} = \frac{-4\pi^2 I\dot{P}}{P^3}} \qquad (6A3)$$

Example: The Crab pulsar has $P = 0.033$ s and $\dot{P} = 10^{-12.4}$. Its rotational energy is changing at the rate

$$\frac{dE_{\rm rot}}{dt} = \frac{-4\pi^2 I \dot{P}}{P^3} = \frac{-4\pi^2 \cdot 10^{45}\ {\rm g\ cm^2} \cdot 10^{-12.4}\ {\rm s\ s^{-1}}}{(0.033\ {\rm s})^3} \approx -4 \times 10^{38}\ {\rm erg\ s^{-1}}$$

Thus the low-frequency (30 Hz) magnetic dipole radiation from the Crab pulsar radiates a huge power $P_{\rm rad} \approx -dE_{\rm rot}/dt \approx 10^5 L_\odot$, comparable with the entire radio output of our Galaxy. It exceeds the Eddington limit, but that is not a problem because the energy *source* is not accretion. It greatly exceeds the average radio pulse luminosity of the Crab pulsar, $\sim 10^{30}$ erg s^{-1}. The long-wavelength magnetic dipole radiation energy is absorbed by and powers the Crab nebula (a "megawave oven").

Figure 3: Composite image of the Crab nebula. Blue indicates X-rays (from Chandra), green is optical (from the HST), and red is radio (from the VLA). Image credit

If we use $-dE_{\rm rot}/dt$ to estimate $P_{\rm rad}$, we can invert Larmor's formula for magnetic dipole radiation to find $B_\perp = B\sin\alpha$ and get a lower limit to the surface magnetic field strength $B > B\sin\alpha$, since we don't generally know the inclination angle α.

$$P_{\rm rad} = -\frac{dE_{\rm rot}}{dt}$$

$$\frac{2}{3c^3}(BR^3\sin\alpha)^2\left(\frac{4\pi^2}{P^2}\right)^2 = \frac{4\pi^2 I\dot{P}}{P^3}$$

$$B^2 = \frac{3c^3 IP\dot{P}}{2\cdot 4\pi^2 R^6\sin^2\alpha}$$

$$B > \left(\frac{3c^3 I}{8\pi^2 R^6}\right)^{1/2}(P\dot{P})^{1/2}$$

Evaluating the constants for the canonical pulsar in cgs units, we get

$$\left[\frac{3 \cdot (3 \times 10^{10}\ \mathrm{cm\ s^{-1}})^3 \cdot 10^{45}\ \mathrm{g\ cm^2}}{8\pi^2 (10^6\ \mathrm{cm})^6}\right]^{1/2} \approx 3.2 \times 10^{19}$$

so the **minimum magnetic field** strength at the pulsar surface is

$$\left(\frac{B}{\mathrm{Gauss}}\right) > 3.2 \times 10^{19} \left(\frac{P\dot{P}}{\mathrm{s}}\right)^{1/2} \quad (6A4)$$

Example: What is the minimum magnetic field strength of the Crab pulsar ($P = 0.033$ s, $\dot{P} = 10^{-12.4}$)?

$$\left(\frac{B}{\text{Gauss}}\right) > 3.2 \times 10^{19} \left(\frac{0.033 \text{ s} \cdot 10^{-12.4}}{\text{s}}\right) = 4 \times 10^{12}$$

This is an amazingly strong magnetic field. Its energy density is

$$U_{\text{B}} = \frac{B^2}{8\pi} > 5 \times 10^{23} \text{ erg cm}^{-3}$$

Just one cm^3 of this magnetic field contains over 5×10^{16} J $= 5 \times 10^{16}$ W s $= 1.6 \times 10^{9}$ W yr of energy, the annual output of a large nuclear power plant. A cubic meter contains more energy than has ever been generated by mankind.

If $(B \sin \alpha)$ doesn't change significantly with time, we can estimate a pulsar's age τ from $P\dot{P}$ by assuming that the pulsar's initial period P_0 was much shorter than the current period. Starting with

$$B^2 = \frac{3c^3 I P \dot{P}}{8\pi^2 R^6 \sin^2 \alpha}$$

we find that

$$P\dot{P} = \frac{8\pi^2 R^6 (B \sin \alpha)^2}{3c^3 I}$$

doesn't change with time. Rewriting the identity $P\dot{P} = P\dot{P}$ as $PdP = P\dot{P}dt$ and integrating over the pulsar's lifetime τ gives

$$\int_{P_0}^{P} PdP = \int_0^{\tau} (P\dot{P})\, dt = P\dot{P} \int_0^{\tau} dt$$

since $P\dot{P}$ is assumed to be constant over time.

$$\frac{P^2 - P_0^2}{2} = P\dot{P}\tau$$

If $P_0^2 \ll P^2$, the ***characteristic age*** of the pulsar is

$$\tau \equiv \frac{P}{2\dot{P}} \qquad (6A5)$$

Note that the characteristic age is not affected by uncertainties in the radius R, moment of inertia I, or $B \sin \alpha$; the only assumptions in its derivation are that $P_0 \ll P$ and that $P\dot{P}$ (i.e. $B \sin\alpha$) is constant.

Example: What is the characteristic age of the Crab pulsar ($P = 0.033$ s, $\dot{P} = 10^{-12.4}$)?

$$\tau = \frac{P}{2\dot{P}} = \frac{0.033 \text{ s}}{2 \cdot 10^{-12.4}} \approx 4.1 \times 10^{10} \text{ s} \approx \frac{4.1 \times 10^{10} \text{ s}}{10^{7.5} \text{ s yr}^{-1}} \approx 1300 \text{ yr}$$

Its actual age is about 950 years.

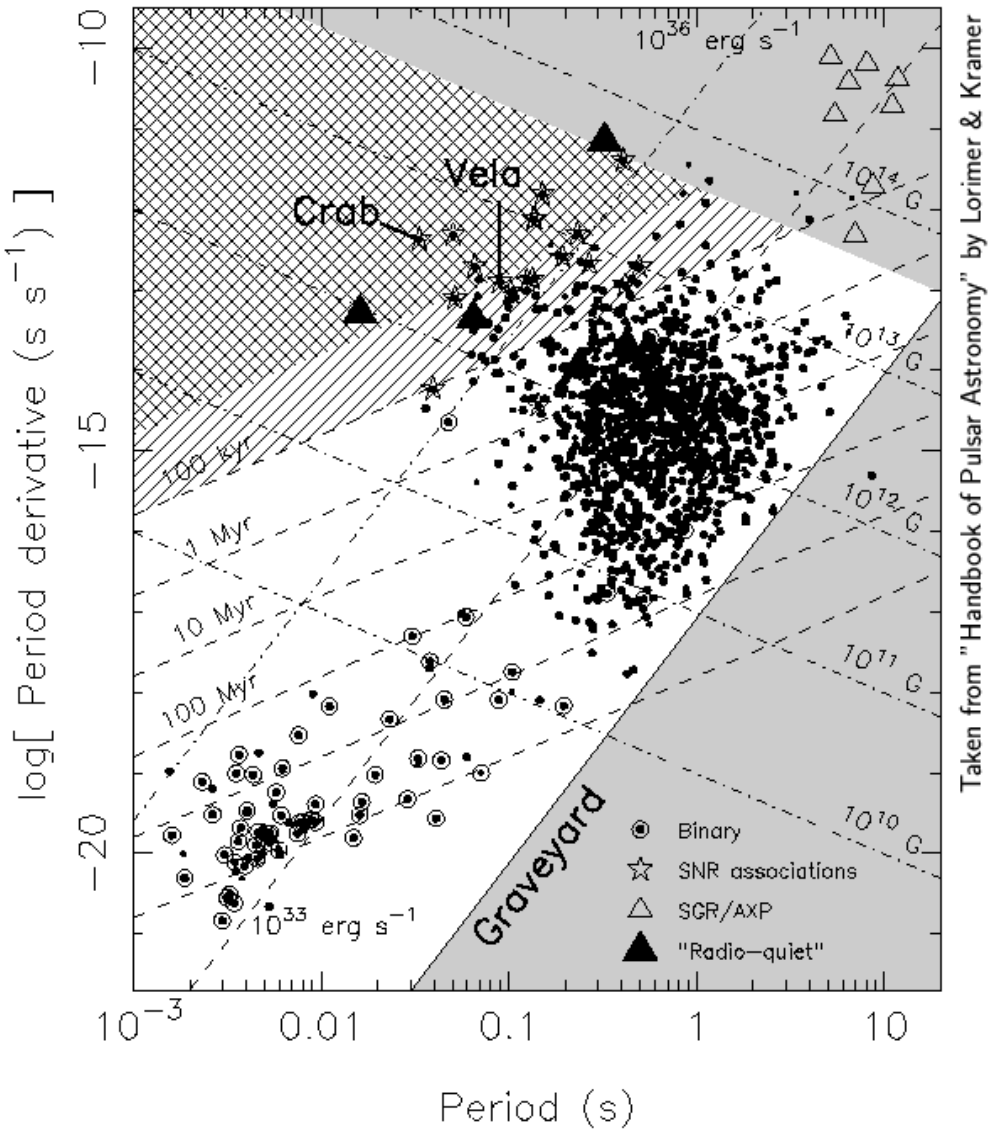

Figure 4: **P-Pdot Diagram**. The $P\dot{P}$ diagram is useful for following the lives of pulsars, playing a role similar to the Hertzsprung-Russell diagram for ordinary stars. It encodes a tremendous amount of information about the pulsar population and its properties, as determined and estimated from two of the primary observables, P and $\dot{P}$. Using those parameters, one can estimate the pulsar age, magnetic field strength B, and spin-down power $\dot{E}$. (From the Handbook of Pulsar Astronomy, by Lorimer and Kramer)

The Lives of Pulsars

Pulsars are born in supernovae and appear in the upper left corner of the $P\dot{P}$ diagram. If B is conserved and they age as described above, they gradually move to the right and down, along lines of constant B and crossing lines of constant characteristic age. Pulsars with characteristic ages $< 10^5$ yr are often found in or near recognizable supernova remnants. Older pulsars are not, either because their SNRs have faded to invisibility or because the supernova explosions expelled the pulsars with enough speed that they have since escaped from their parent SNRs. The bulk of the pulsar population is older than 10^5 yr but much younger than the Galaxy ($\sim 10^{10}$ yr). The observed distribution of pulsars in the $P\dot{P}$ diagram indicates that something changes as pulsars age. One controversial possibility is that the magnetic fields of old pulsars must decay on time scales $\sim 10^7$ yr, causing old pulsars to move almost straight down in the $P\dot{P}$ diagram until they fall below into the graveyard below the ***death line*** and cease radiating radio pulses.

Almost all short-period pulsars below the ***spin-up line*** near $\log[\dot{P}/P(\mathrm{sec})] \approx -16$ are in binary systems, as evidenced by periodic (i.e. orbital) variations in their observed pulse periods. These ***recycled pulsars*** have been spun up by accreting mass and angular momentum from their companions, to the point that they emit radio pulses despite their relatively low magnetic field strengths $B \sim 10^8$ G (the accretion causes a substantial reduction in the magnetic field strength). The magnetic fields of neutron stars funnel ionized accreting material onto the magnetic polar caps, which become so hot that they emit X-rays. As the neutron stars rotate, the polar caps appear and disappear from view, causing periodic fluctuations in X-ray flux; many are detectable as X-ray pulsars.

Millisecond pulsars (MSPs) with low-mass ($M \sim 0.1 - 1 M_{\odot}$) white-dwarf companions typically have orbits with small eccentricities. Pulsars with extremely eccentric orbits usually have neutron-star companions, indicating that these companions also exploded as supernovae and nearly disrupted the binary system. Stellar interactions in globular clusters cause a much higher fraction of recycled pulsars per unit mass than in the Galactic disk. These interactions can result in very strange systems such as pulsar–main-sequence-star binaries and MSPs in highly eccentric orbits. In both cases, the original low-mass companion star that recycled the pulsar was ejected in an interaction and replaced by another star. (The ***eccentricity*** e of an elliptical orbit is defined as the ratio of the separation of the foci to the length of the major axis. It ranges between $e = 0$ for a circular orbit and $e = 1$ for a parabolic orbit.)

A few millisecond pulsars are isolated. They were probably recycled via the standard scenario in binary systems, but the energetic millisecond pulsars eventually ablated their companions away.

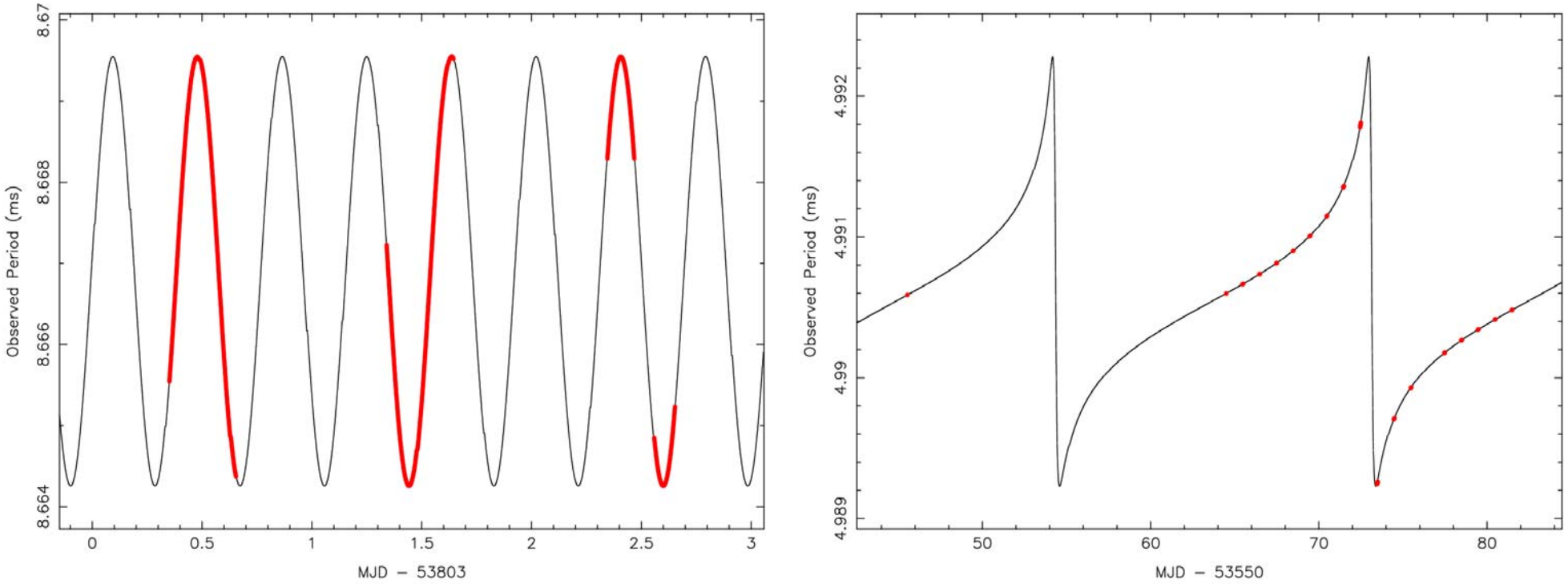

Figure 5: Examples of Doppler variations observed in binary systems containing pulsars. (left) The Doppler variations of the globular cluster MSP J1748−2446N in Terzan 5. This pulsar is in a nearly circular orbit (eccentricity $e = 4.6 \times 10^{-5}$) with a companion of minimum mass 0.47 $M_\odot$. The difference between the semi-major and semi-minor axes for this orbit is only 51±4 cm! The thick red lines show the periods as measured during GBT observations. (right) Similar Doppler variations from the highly eccentric binary MSP J0514−4002A in the globular cluster NGC 1851. This pulsar has one of the most eccentric orbits known ($e = 0.888$) and a massive white dwarf or neutron-star companion.

Emission Mechanisms

The radio pulses originate in the pulsar magnetosphere. Because the neutron star is a spinning magnetic dipole, it acts as a ***unipolar generator***. The total Lorentz force acting on a charged particle is

$$\vec{F} = q\left(\vec{E} + \frac{\vec{v} \times \vec{B}}{c}\right) .$$

Charges in the magnetic equatorial region redistribute themselves by moving along closed field lines until they build up an electrostatic field large enough to cancel the magnetic force and give $|\vec{F}| = 0$. The voltage induced is about 10^{16} V in MKS units. However, the co-rotating field lines emerging from the polar caps cross the ***light cylinder*** (the cylinder centered on the pulsar and aligned with the rotation axis at whose radius the co-rotating speed equals the speed of light) and these field lines cannot close. Electrons in the polar cap are magnetically accelerated to very high energies along the open but curved field lines, where the acceleration resulting from the curvature causes them to emit ***curvature radiation*** that is strongly polarized in the plane of curvature. As the radio beam sweeps across the line-of-sight, the plane of polarization is observed to rotate by up to 180 degrees, a purely geometrical effect.

High-energy photons produced by curvature radiation interact with the magnetic field and lower-energy photons to produce electron-positron pairs that radiate more high-energy photons. The final results of this cascade process are bunches of charged particles that emit at radio wavelengths. The death line in the $P\dot{P}$ diagram corresponds to neutron stars with sufficiently low B and high P that the curvature radiation near the polar surface is no longer capable of generating particle cascades. The extremely high brightness temperatures are explained by **coherent radiation**. The electrons do not radiate as independent charges e; instead bunches of N electrons in volumes whose dimensions are less than a wavelength emit in phase as charges Ne. Since Larmor's formula indicates that the power radiated by a chage q is proportional to q^2, the radiation intensity can be N^2 times brighter than incoherent radiation from the same total number N of electrons. Because the coherent volume is smaller at shorter wavelengths, most pulsars have extremely steep radio spectra. Typical (negative) pulsar spectral indices are $\alpha \sim$1.7 ($S \propto \nu^{-1.7}$), although some can be much steeper ($\alpha > 3$) and a handful are almost flat ($\alpha < 0.5$).

Pulsars and the Interstellar Medium

(Note: the following closely follows the discussion in the *Handbook of Pulsar Astronomy* by Lorimer and Kramer)
With their sharp and short-duration pulse profiles and very high brightness temperatures, pulsars are unique probes of the interstellar medium (ISM). The electrons in the ISM make up a cold plasma having a refractive index

$$\mu = \left[1 - \left(\frac{\nu_{\rm p}}{\nu}\right)^2\right]^{1/2},$$

where ν is the frequency of the radio waves, $\nu_{\rm p}$ is the ***plasma frequency***

$$\nu_{\rm p} = \left(\frac{e^2 n_{\rm e}}{\pi m_{\rm e}}\right)^{1/2} \approx 8.97\ {\rm kHz} \times \left(\frac{n_{\rm e}}{\rm cm^{-3}}\right)^{1/2} \quad (6A6)$$

and $n_{\rm e}$ is the electron number density. For a typical ISM value $n_{\rm e} \sim 0.03$ cm^{-3}, $\nu_{\rm p} \sim 1.5$ kHz. If $\nu < \nu_{\rm p}$ then μ is imaginary and radio waves cannot propagate through the plasma.

For propagating radio waves, $\mu < 1$ and the ***group velocity*** $v_g = \mu c$ of pulses is less than the vacuum speed of light. For most radio observations $\nu_p \ll \nu$ so

$$v_g \approx c\left(1 - \frac{\nu_p^2}{2\nu^2}\right) \quad (6A7)$$

A broadband pulse moves through a plasma more slowly at lower frequencies than at higher frequencies. If the distance to the source is d, the ***dispersion delay*** t at frequency ν is

$$t = \int_0^d v_g^{-1} dl - \frac{d}{c} = \frac{1}{c}\int_0^d \left(1 + \frac{\nu_p^2}{2\nu^2}\right) dl - \frac{d}{c}$$

$$= \frac{e^2}{2\pi m_e c} \frac{\int_0^d n_e dl}{\nu^2}.$$

In astronomically convenient units this becomes

$$\left(\frac{t}{\text{sec}}\right) \approx 4.149 \times 10^3 \left(\frac{\text{DM}}{\text{pc cm}^{-3}}\right)\left(\frac{\nu}{\text{MHz}}\right)^{-2} \quad \text{(6A8)}$$

where

$$\text{DM} \equiv \int_0^d n_e dl \quad \text{(6A9)}$$

in units of pc cm^{-3} is called the ***dispersion measure***.

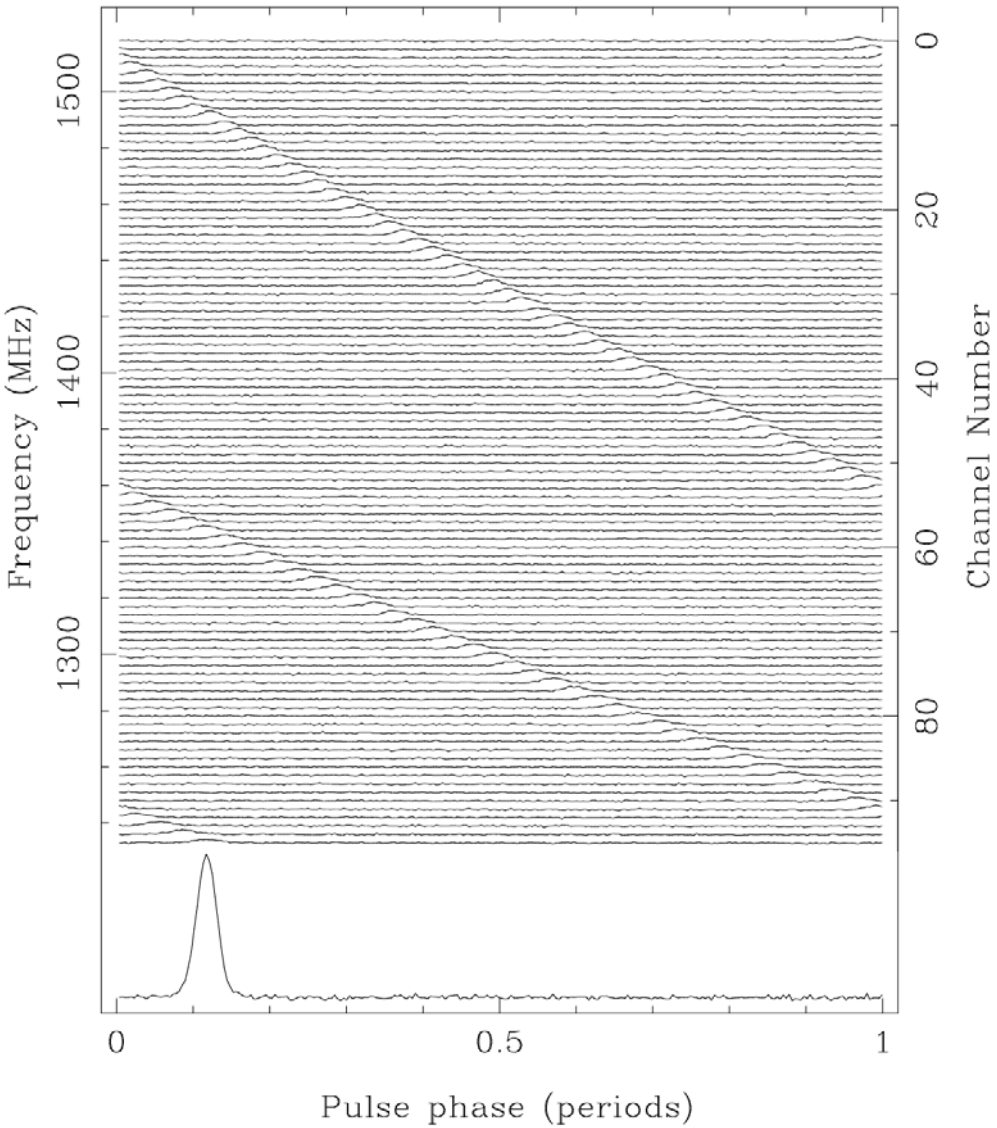

Figure 6: Pulsar dispersion. Uncorrected dispersive delays for a pulsar observation over a bandwidth of 288 MHz (96 channels of 3 MHz width each), centered at 1380 MHz. The delays wrap *since the data are folded (i.e. averaged) modulo the pulse period. (From the* Handbook of Pulsar Astronomy, *by Lorimer and Kramer)*

Measurements of the dispersion measure can provide distance estimates to pulsars. Crude estimates can be made for pulsars near the Galactic plane assuming that $n_e \sim 0.03$ cm^{-3}. However, several sophisticated models of the Galactic electron-density distribution now exist (e.g. NE2001; Cordes & Lazio 2002, astro-ph/0207156) that can provide much better ($\Delta d/d \sim 30\%$) distance estimates.

Since pulsar observations almost always cover a wide bandwidth, uncorrected differential delays across the band will cause ***dispersive smearing*** of the pulse profile. For pulsar searches, the DM is unknown and becomes a search parameter much like the pulsar spin frequency. This extra search dimension is one of the primary reasons that pulsar searches are computationally intensive.

Besides directly determining the integrated electron density along the line of site, observations of pulsars can be used to probe the ISM via absorption by spectral lines of HI or molecules (which can be used to estimate the pulsar distance as well), scintillation (allowing estimates of the pulsar transverse velocity), and pulse broadening.

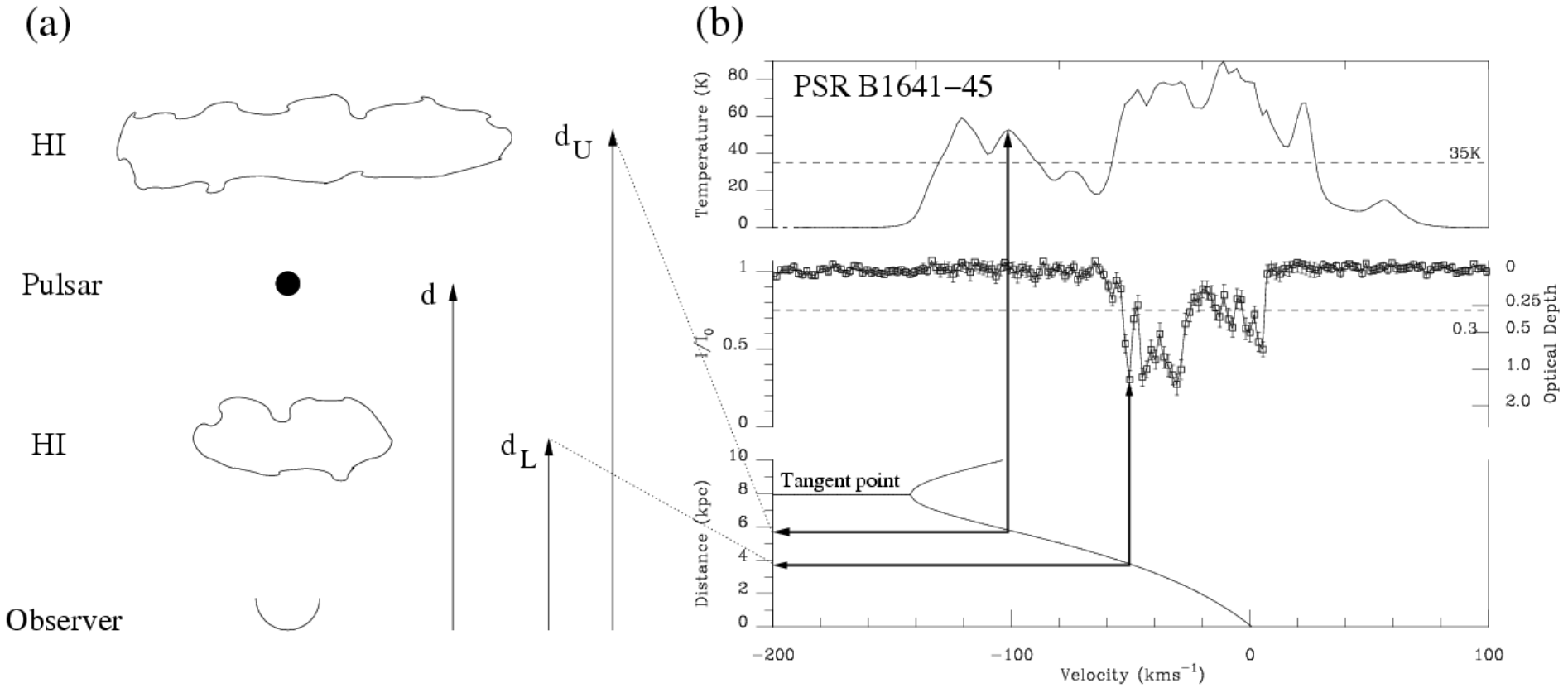

Figure 7: Pulsar HI Absorption Measurement. With a model for the Galactic rotation, such absorption measurements can provide pulsar distance estimates or constraints. (From the Handbook of Pulsar Astronomy*, by Lorimer and Kramer)*

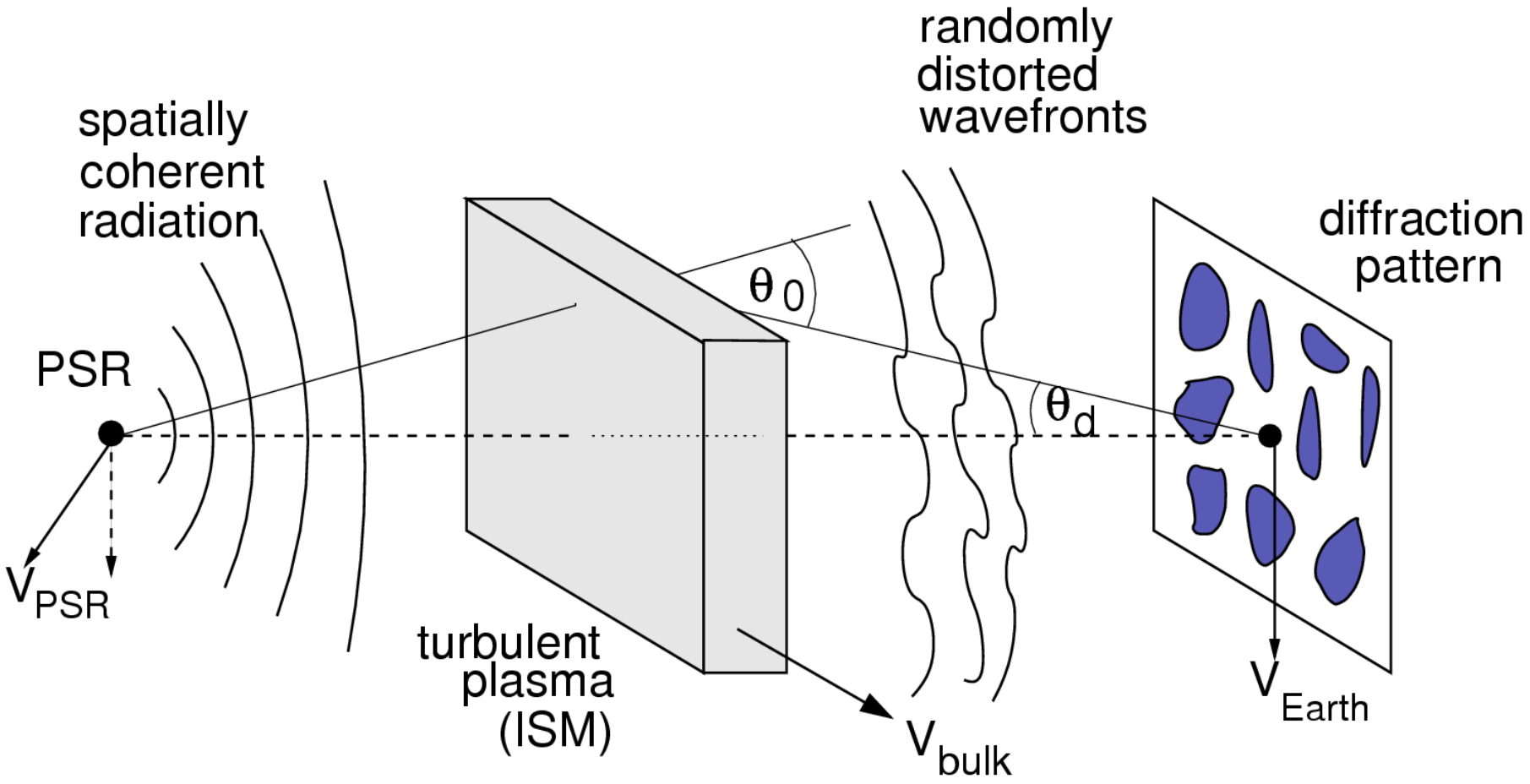

Figure 8: Thin Screen Diffraction/Scattering model. Inhomogeneities in the ISM cause small-angle deviations in the paths of the radio waves. These deviations result in time (and therefore phase) delays that can interfere to create a diffraction pattern, broaden the pulses in time, and make a larger image of the pulsar on the sky. (From the Handbook of Pulsar Astronomy*, by Lorimer and Kramer)*

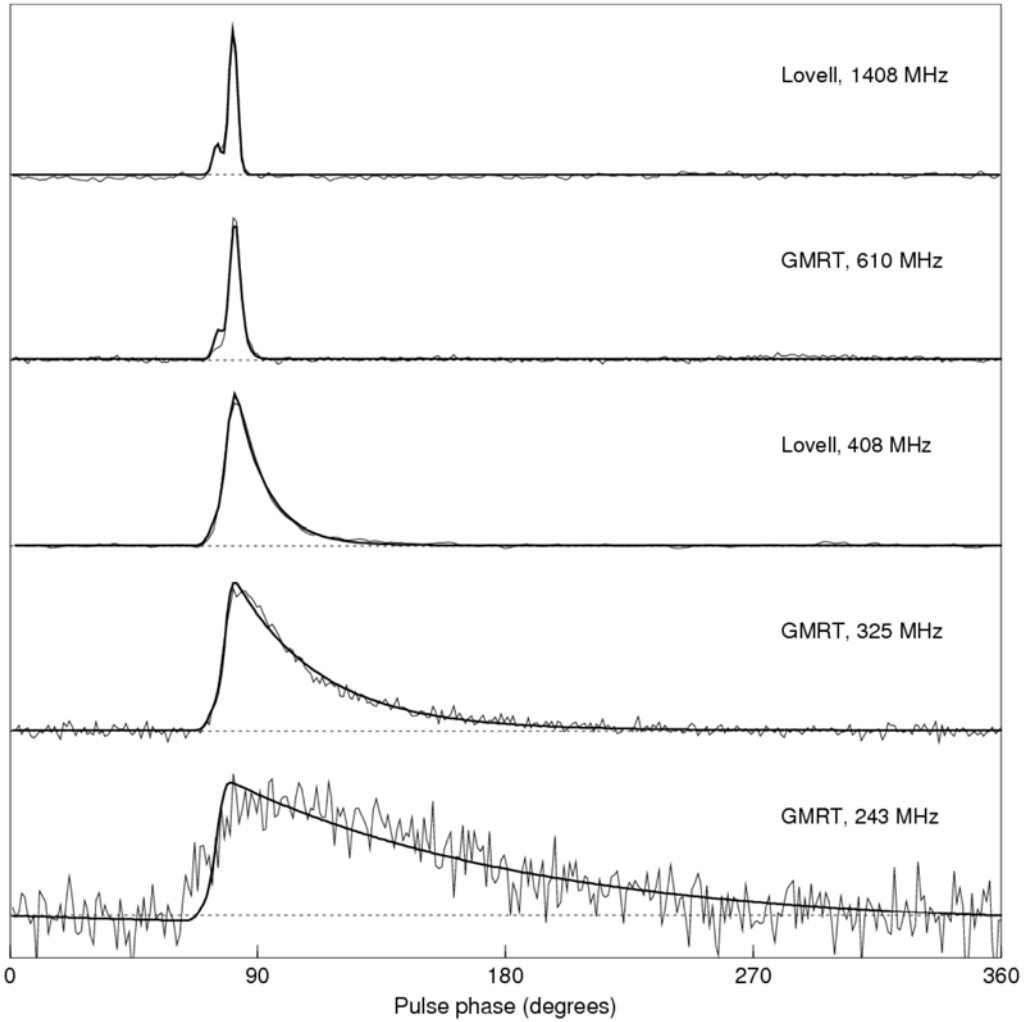

Figure 9: Pulse broadening caused by scattering. Scattering of the pulsed signal by ISM inhomogeneities results in delays that cause a scattering tail. This scatter-broadening can greatly decrease both the observational sensitivity and the timing precision for such pulsars.

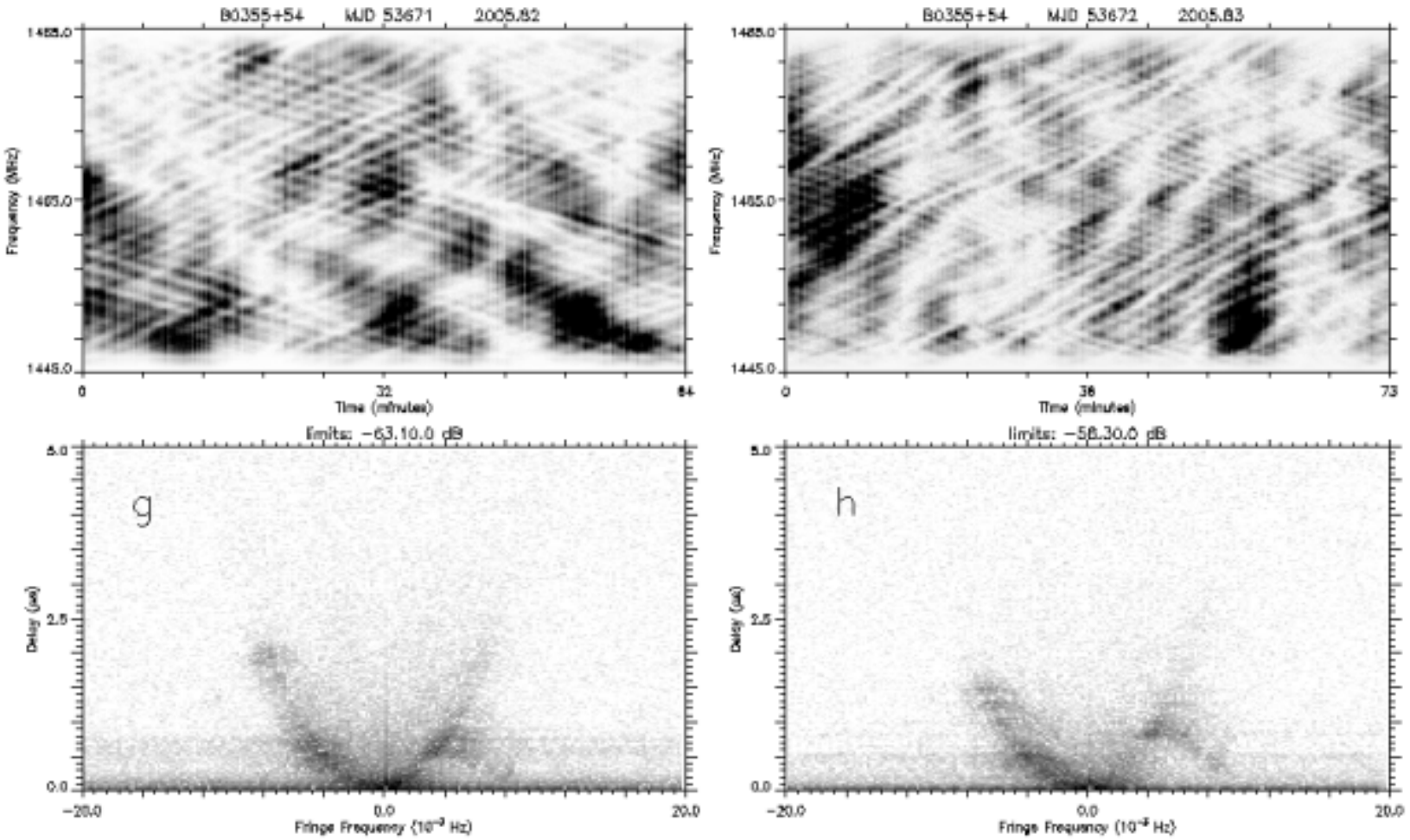

Figure 10: Diffractive Scintillation of a Pulsar. The top plots show dynamic spectra of the bright pulsar B0355+54 taken on two consecutive days with the GBT. The bottom plots show the so-called secondary spectra (the Fourier transforms of the dynamic spectra) and the so-called scintillation arcs (and moving arclets). (Figure provided by Dan Stinebring; who will join UvA on his sabbatical end 2013)

Pulsar Timing

Pulsars are intrinsically interesting and exotic objects, but much of the best science based on pulsar observations has come from their use as *tools* via pulsar timing. Pulsar timing is the regular monitoring of the rotation of the neutron star by tracking (nearly exactly) the times of arrival of the radio pulses. The key point to remember is that *pulsar timing unambiguously accounts for every single rotation of the neutron star over long periods (years to decades) of time*. This unambiguous and very precise tracking of rotational phase allows pulsar astronomers to probe the interior physics of neutron stars, make extremely accurate astrometric measurements, and test gravitational theories in the strong-field regime in unique ways.

For pulsar timing, astronomers "fold" radio data modulo the instantaneous pulse period P or pulse frequency $f = 1/P = d\phi/dt$. Averaging over many pulses yields a high signal-to-noise average pulse profile. Although individual pulse shapes vary considerably, the shape of the average profile is quite stable. Typically, the average profile is correlated with a template or model profile so that a phase offset can be determined. When multiplied by the instantaneous pulse period, that phase yields a time offset that can be added to a high-precision reference point on the profile (for example, the left edge of the profile based on the recorded time of the first sample of the observation) to create the time-of-arrival or ***TOA***. The precision with which a TOA can be determined is approximately equal to the duration of a sharp pulse feature (e.g., the leading edge) divided by the signal-to-noise ratio of the average profile. It is usually expressed in terms of the width of the pulse features W_f in units of the period P, the pulse period P, and the signal-to-noise ratio SNR such that $\sigma_{\mathrm{TOA}} \propto W_f P/\mathrm{SNR}$. Therefore strong, fast pulsars with narrow pulse profiles provide the best arrival times.

In the nearly inertial frame of the Solar-system barycenter, the rotational period of a pulsar is nearly constant, so the time-dependent phase $\phi(t)$ of a pulsar can be approximated by a Taylor expansion

$$\phi(t) = \phi_0 + f(t - t_0) + \frac{1}{2}\dot{f}(t - t_0)^2 + \ldots,$$

where ϕ_0 and t_0 are arbitrary reference phases and times for each pulsar. The important thing about pulsar timing, though, is that the observed rotational phase difference between each of the TOAs must contain an integer number of rotations. Since each TOA corresponds to a different time t, the parameters that we are fitting for, such as f and $\dot{f}$, must result in a phase change between each pair of TOAs i and j that is an integer number of turns, or $\Delta\phi_{ij} = n$ turns (1 turn = 2π radians). Since all measurements are made with regard to the integrated pulse *phase* rather than the instantaneous pulse period, the precision with which astronomers can make long-term timing measurements can be quite extraordinary.

Example: With what precision can we determine the spin frequency f of a pulsar using pulsar timing?

Since $f = d\phi/dt$ when ϕ is measured in turns, the precision is based on how precisely we can measure a change in phase $\Delta\phi$ over some time interval ΔT. Typically, ΔT is a long period of time (up to several tens of years for many pulsars now) over which a pulsar's phase has been tracked through regular monitoring. $\Delta\phi$ is determined principally by the individual TOA precisions, although for some types of measurments a statistical component is important as well since precision improves as the number of measurements $N^{-1/2}$ if the random errors are larger than the systematic errors.

For the original millisecond pulsar B1937+21, the TOA precision is approximately 1 μs (which is a fractional error in phase of about 6×10^{-4} turns, and it has been timed for over 25 years:

$$\Delta f \sim \frac{\sigma_{\rm TOA}}{\Delta T} = \frac{6 \times 10^{-4}}{25\,{\rm yrs} \times 3.15 \times 10^7 {\rm s\,yr}^{-1}} = 8 \times 10^{-13}\,{\rm Hz}.$$

In order to measure $\phi(t)$ in this form, though, many corrections have to be applied to the observed TOAs first. If we measure a pulse at our observatory on Earth at topocentric (***topocentric*** means measured from a fixed point on the Earth's surface) time $t_{\rm t}$, we can correct this time to the time t in the nearly inertial Solar-system center of mass or ***barycentric frame***, which we assume to be the nearly the same as the time in the frame comoving with the pulsar. Note that the measured pulse rates will differ from the actual pulse rates in the pulsar frame by the unknown Doppler factor resulting from the unknown line-of-sight pulsar velocity.

$$t = t_{\rm t} - t_{t_0} + \Delta_{\rm clock} - \Delta_{\rm DM} + \Delta_{\rm R\odot} + \Delta_{\rm E\odot} + \Delta_{\rm S\odot} + \Delta_{\rm R} + \Delta_{\rm E} + \Delta_{\rm S}.$$

As before, t_{t_0} is a reference epoch, $\Delta_{\rm clock}$ represents clock correction that accounts for differences between the observatory clocks and terrestrial time standards, $\Delta_{\rm DM}$ is the dispersion delay caused by the ISM, and the other Δ terms are delays from within the Solar System and, if the pulsar is in a binary, from within its orbit. The ***Roemer delay*** $\Delta_{\rm R\odot}$ is the classical light travel time across the Earth's orbit, with a magnitude of $\sim 500 \cos\beta$ s, where β is the ecliptic latitude of the pulsar, and $\Delta_{\rm R}$ is the corresponding delay across the orbit of a pulsar in a binary or multiple system. The ***Einstein delay*** $\Delta_{\rm E}$ accounts for the time dilation from the moving pulsar (and observatory) and the gravitational redshift caused by the Sun and planets or the binary companion, and the ***Shapiro delay*** $\Delta_{\rm S}$ is the extra time required by the pulses to travel through the curved space-time containing the Sun/planets/companions. Errors in any of these parameters, as well as other parameters such as f, $\dot{f}$, and proper motion, give very specific systematic signatures in plots of the ***timing residuals***, which are simply the phase differences between the observed TOAs and the predicted TOA times based on the current model parameters.

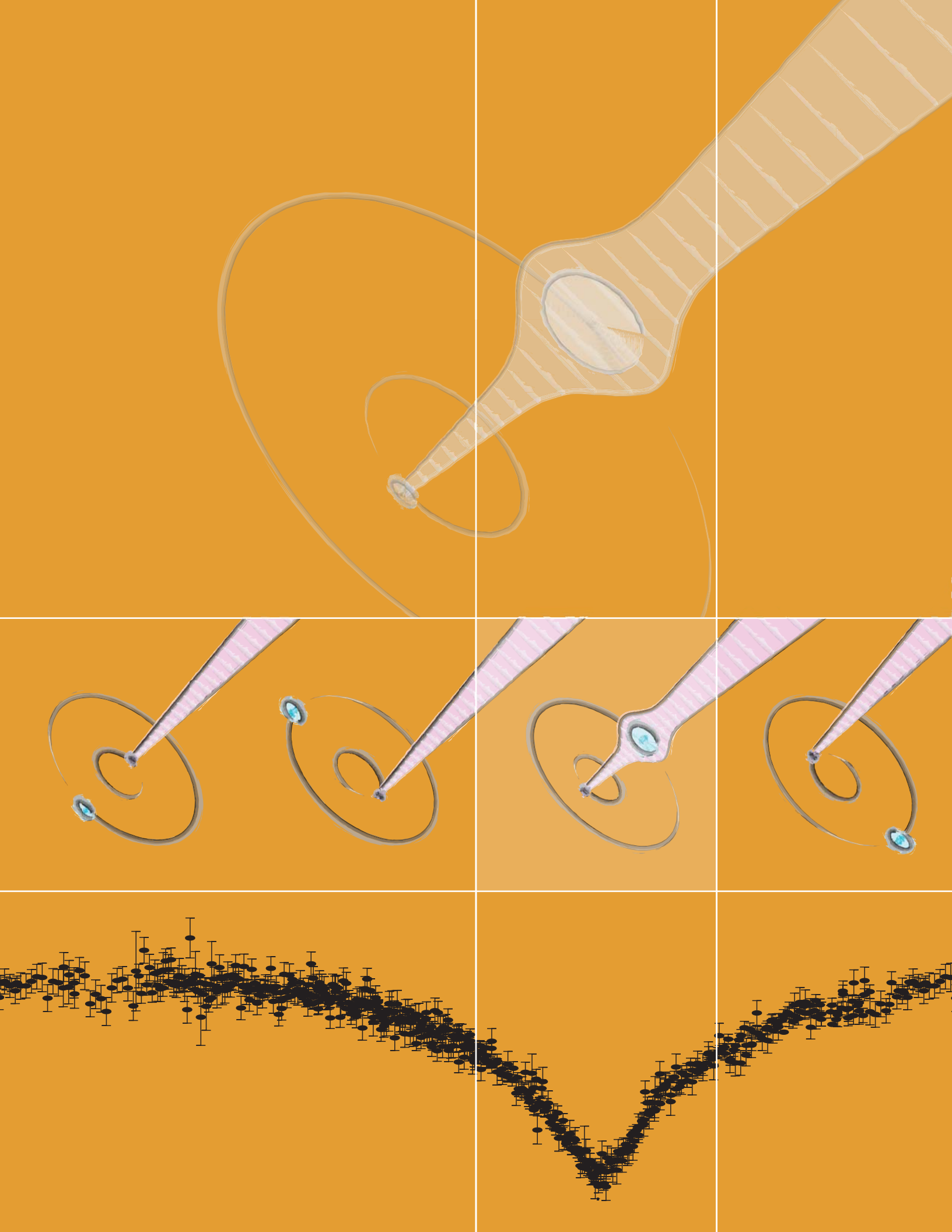

Example: How (and how accurately) can we measure positions using pulsar timing?

Pulsar positions on the sky are determined by timing a pulsar over the course of a year as the Earth orbits the Sun and tracking the changing time delays (i.e. the Roemer delay) of pulses as the Earth moves.

The Roemer delay τ across the Solar System from a pulsar at ecliptic coordinates λ (longitude) and β (latitude) is:

$$\tau \simeq 500\,\mathrm{s}\ \cos(\beta)\cos\left(\theta(t)+\lambda\right),$$

where $\theta(t)$ is the orbital phase of the Earth with respect to the vernal equinox. This is an approximate time delay since we are assuming that the Earth's orbit is circular.

If there is an error in our position estimate, the individual position errors components $\Delta\lambda$ and $\Delta\beta$ cause a differential time delay $\Delta\tau$ to be present in the timing residuals with respect to the correct Roemer delay:

$$\Delta\tau \simeq 500\,\mathrm{s}\ \left[\cos(\beta+\Delta\beta)\cos\left(\theta(t)+\lambda+\Delta\lambda\right)-\cos(\beta)\cos(\theta(t)+\lambda)\right].$$

If the positional errors are small, such that we can use $\sin x \sim x$, $\cos x \sim 1$, and $\Delta\beta\,\Delta\lambda \sim 0$, we can use trigonometric angle-sum identities and then simplify to get:

$$\Delta\tau \simeq -500\,\mathrm{s}\ \left[\Delta\lambda\cos(\beta)\sin(\theta(t)+\lambda)+\Delta\beta\sin(\beta)\cos\left(\theta(t)+\lambda\right)\right].$$

Comparing the trig identity $A\sin\left(\theta(t)+\phi\right)=A\cos\phi\sin\theta(t)+A\sin\phi\cos\theta(t)$ to the equation for $\Delta\tau$, we see that:

$$A\cos\phi = -500\,\mathrm{s}\;\Delta\lambda\cos\beta$$

$$A\sin\phi = -500\,\mathrm{s}\;\Delta\beta\sin\beta,$$

and therefore:

$$\Delta\lambda = -\frac{A\cos\phi}{500\,\mathrm{s}\;\cos\beta}$$

$$\Delta\beta = -\frac{A\sin\phi}{500\,\mathrm{s}\;\sin\beta},$$

where A and ϕ are the amplitude and phase of the error sinusoid in the timing residuals.

When the pulsar is located near the ecliptic plane (with $\beta \sim 0$), $\cos\beta \sim 1$ and there is maximum timing leverage (and therefore minimum error) to determine λ. However, $\sin\beta \sim 0$ and so the errors on β are huge. If astrometric accuracy for pulsars near the ecliptic is necessary, VLBI positions are the best way to go.

For the timing fits themselves, the amplitude of the sinusoid A is in time units (i.e. light travel time) and a timing fit will determine A to an absolute precision ΔA approximately equal to the TOA uncertainty. If that uncertainty is small, say 2 μs for a millisecond pulsar, and there are a large number of measurements (say $N = 16$) over the course of a year, the averaged phase errors (and therefore the errors on A) will be approximately $\sim 2\,\mu s/\sqrt{16} \sim 5 \times 10^{-7}$ sec. The overall position errors for an MSP 30° off the ecliptic plane are approximately

$$\Delta\lambda \sim \frac{5 \times 10^{-7}}{500\;\cos\beta} = 1 \times 10^{-9}\,\mathrm{radians}$$

and

$$\Delta\beta \sim \frac{5 \times 10^{-7}}{500 \, \sin\beta} = 2 \times 10^{-9} \, \mathbf{radians.}$$

These correspond to errors in both directions of only a few hundred micro-arcsec! Even normal pulsars with slow spin periods provide astrometric precisions typically of 0.1 arcsec or better.

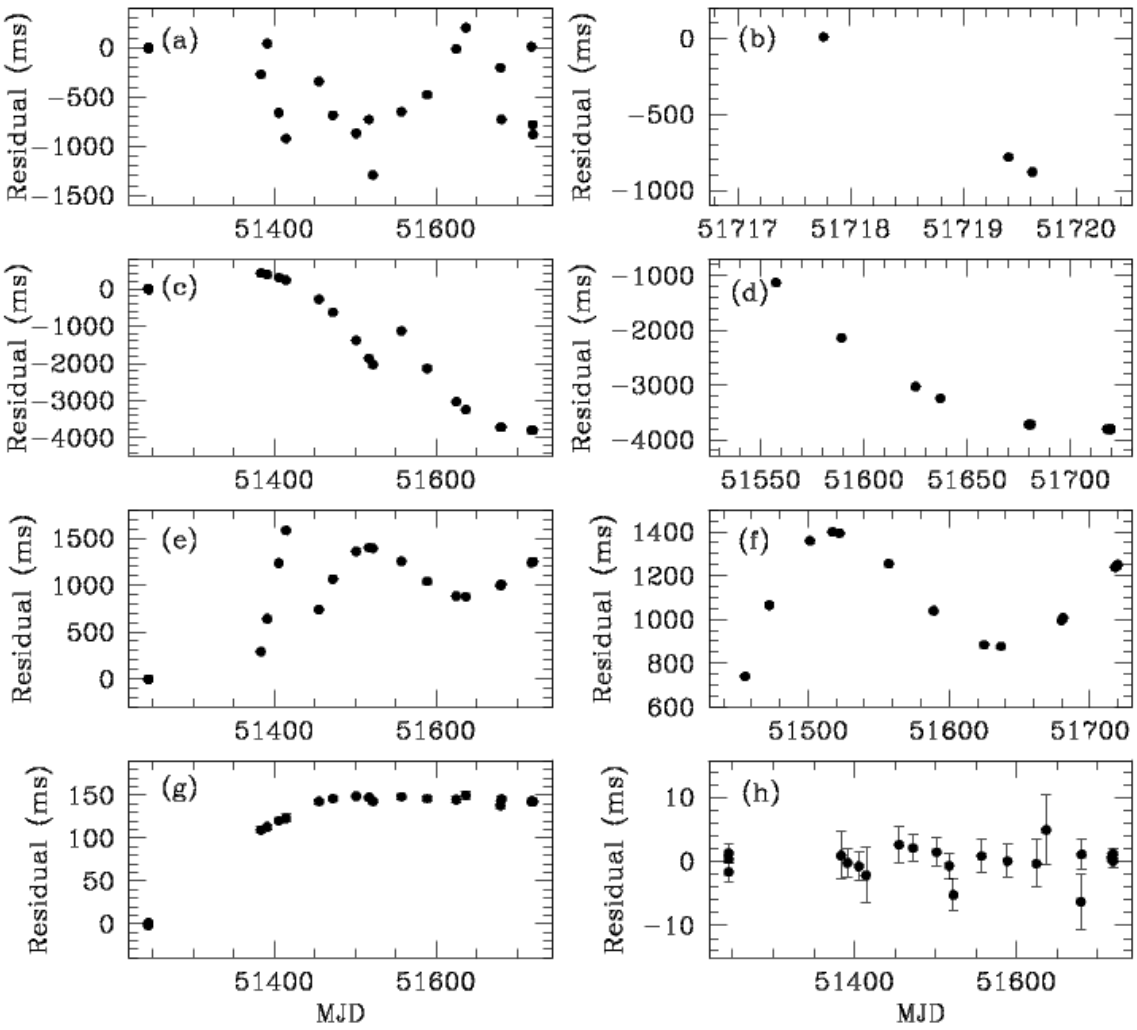

Figure 1: Establishing a timing solution for an isolated pulsar. In panel (e), you identify closely spaced days with unambiguous phase connection and fit for spin frequency. In panel (f), you extend that phase connection until either RA or Dec errors dominate and then fit for it. In panel (g), you fit for the other position component. Finally, in panel (h), you fit for frequency derivative, which completes the timing solution.

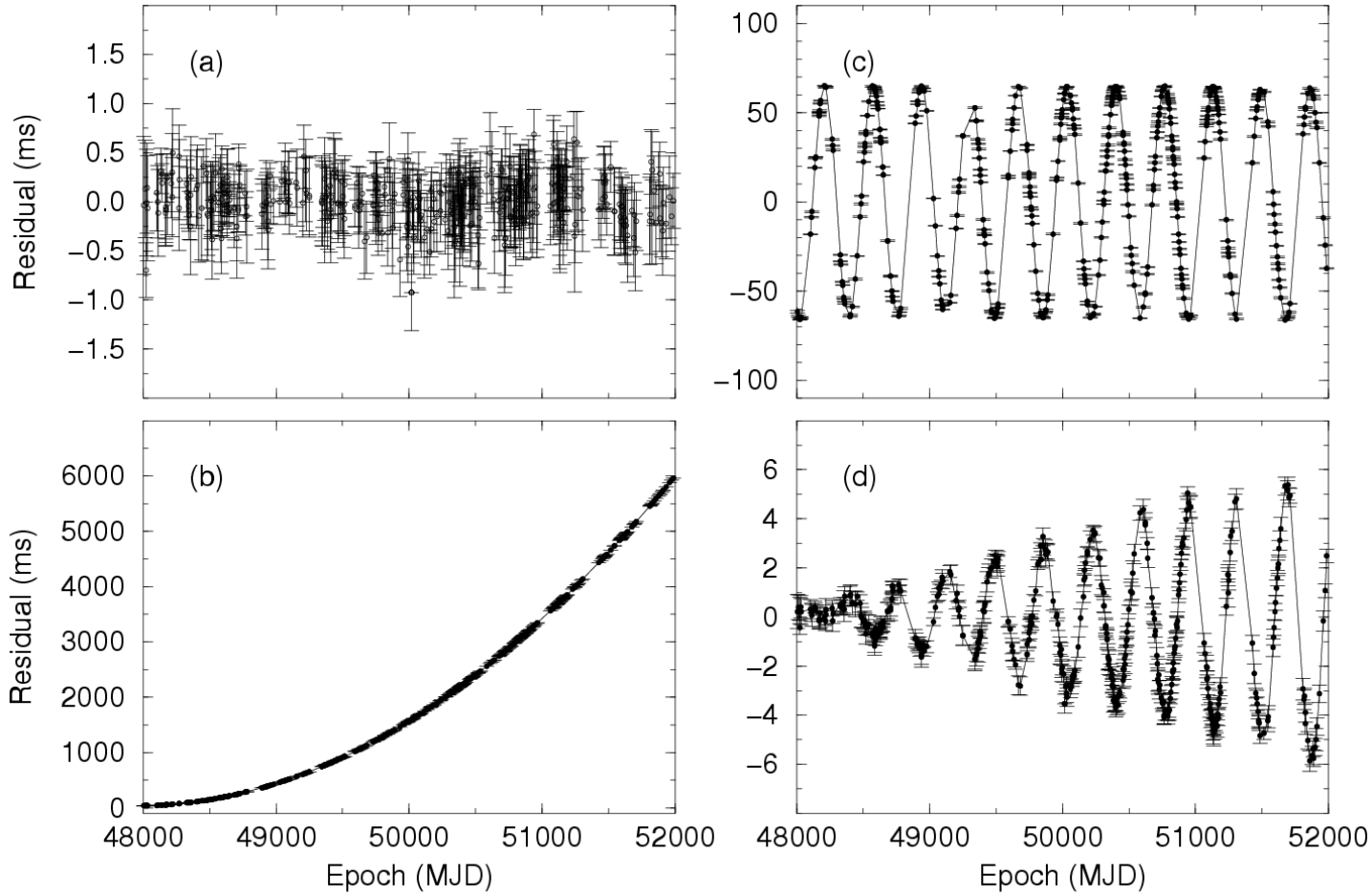

Figure 2: Pulsar timing examples. Panel (a) shows a "good" timing solution with no unmodeled effects. The sinusoidal ripple in Panel (c) indicates an error in position. Panel (b) shows an error in the frequency derivative ($f = d\phi/dt$ so $\dot{f} = d^2\phi/dt^2$). Panel (d) shows unmodeled pulsar proper motion.

For binary pulsars, the pulsar Roemer delays comprise up to five Keplerian parameters: the projected semi-major axis $x \equiv a_1 \sin i/c$, the longitude of periastron ω, the time of periastron passage T_0, the orbital period P_b, and the orbital eccentricity e. Relativistic binaries may allow the measurement of up to 5 ***post-Keplerian (PK) parameters***: the rate of periastron advance $\dot{\omega}$, the orbital period decay $\dot{P}_b$, the so-called relativistic γ (i.e. the Einstein term corresponding to time dilation and gravitational redshift), and the Shapiro delay terms r (range) and s (shape).

Table 1 PSR J0437–4715 physical parameters

Right ascension, α (J2000) ...	$04^{\rm h}37^{\rm m}15\overset{\rm s}{.}7865145(7)$
Declination, δ (J2000)	-47°15′08″.461584(8)
μ_α (mas yr^{-1})	121.438(6)
μ_δ (mas yr^{-1})	-71.438(7)
Annual parallax, π (mas)	7.19(14)
Pulse period, P (ms)	5.757451831072007(8)
Reference epoch (MJD)	51194.0
Period derivative, $\dot{P}$ (10^{-20}) ..	5.72906(5)
Orbital period, $P_{\rm b}$ (days)	5.741046(3)
x (s)	3.36669157(14)
Orbital eccentricity, e	0.000019186(5)
Epoch of periastron, T_0 (MJD)	51194.6239(8)
Longitude of periastron, ω (°) .	1.20(5)
Longitude of ascension, Ω (°) .	238(4)
Orbital inclination, i (°)	42.75(9)
Companion mass, m_2 ($M_\odot$) ...	0.236(17)
$\dot{P}_{\rm b}(10^{-12})$	3.64(20)
$\dot{\omega}$ (°yr^{-1})	0.016(10)

Table 1: Millisecond pulsar timing example. A timing ephemeris for the nearby MSP J0437−4715 by van Straten et al. 2001. This is one of the best "timing" pulsars known (post-fit RMS timing residuals of ∼100 ns), and this measurement is one of the most accurate astrometric measurements ever made. In addition, the timing accuracy allowed a fundamentally new test of general relativity.

In any theory of gravity, the five PK parameters are functions only of the pulsar mass m_1, the companion mass m_2, and the standard five Keplerian orbital parameters. For general relativity, the formulas are:

$$\dot{\omega} = 3 \left(\frac{P_b}{2\pi} \right)^{-5/3} (T_\odot M)^{2/3} (1 - e^2)^{-1}$$

$$\gamma = e \left(\frac{P_b}{2\pi} \right)^{1/3} T_\odot^{2/3} M^{-4/3} m_2 (m_1 + 2m_2)$$

$$\dot{P}_b = -\frac{192\pi}{5} \left(\frac{P_b}{2\pi} \right)^{-5/3} \left(1 + \frac{73}{24} e^2 + \frac{37}{96} e^4 \right) (1 - e^2)^{-7/2} T_\odot^{5/3} m_1 m_2 M^{-1/3}$$

$$r = T_\odot m_2$$

$$s = x \left(\frac{P_b}{2\pi} \right)^{-2/3} T_\odot^{-1/3} M^{2/3} m_2^{-1}.$$

In these equations, $T_\odot \equiv GM_\odot/c^3 = 4.925490947\,\mu$s is the solar mass in time units, m_1, m_2, and $M \equiv m_1 + m_2$ are in solar masses, and $s \equiv \sin i$ (where i is the orbital inclination). If any two of these PK parameters are measured, the masses of the pulsar and its companion can be determined. If more than two are measured, each additional PK parameter yields a different test of a gravitational theory.

For the famous case of the Hulse-Taylor binary pulsar B1913+16, high-precision measurements of $\dot{\omega}$ and γ were first made to determine the masses of the two neutron stars accurately. The Nobel-prize-winning measurement came with the eventual detection of $\dot{P}_b$, which implied that the orbit was decaying in accordance with general relativity's predictions for the the emission of gravitational radiation. The recently discovered double-pulsar system J0737−3039 is in a more compact orbit (2.4 hrs compared to 7.7 hrs for PSR B1913+16), which allows the measurement of all five PK parameters as well as the mass ratio R, giving a total of four tests of general relativity. Kramer et al. (2006) showed that GR is correct at the 0.05% level and measured the masses of the two neutron stars to better than 1 part in 10^4.

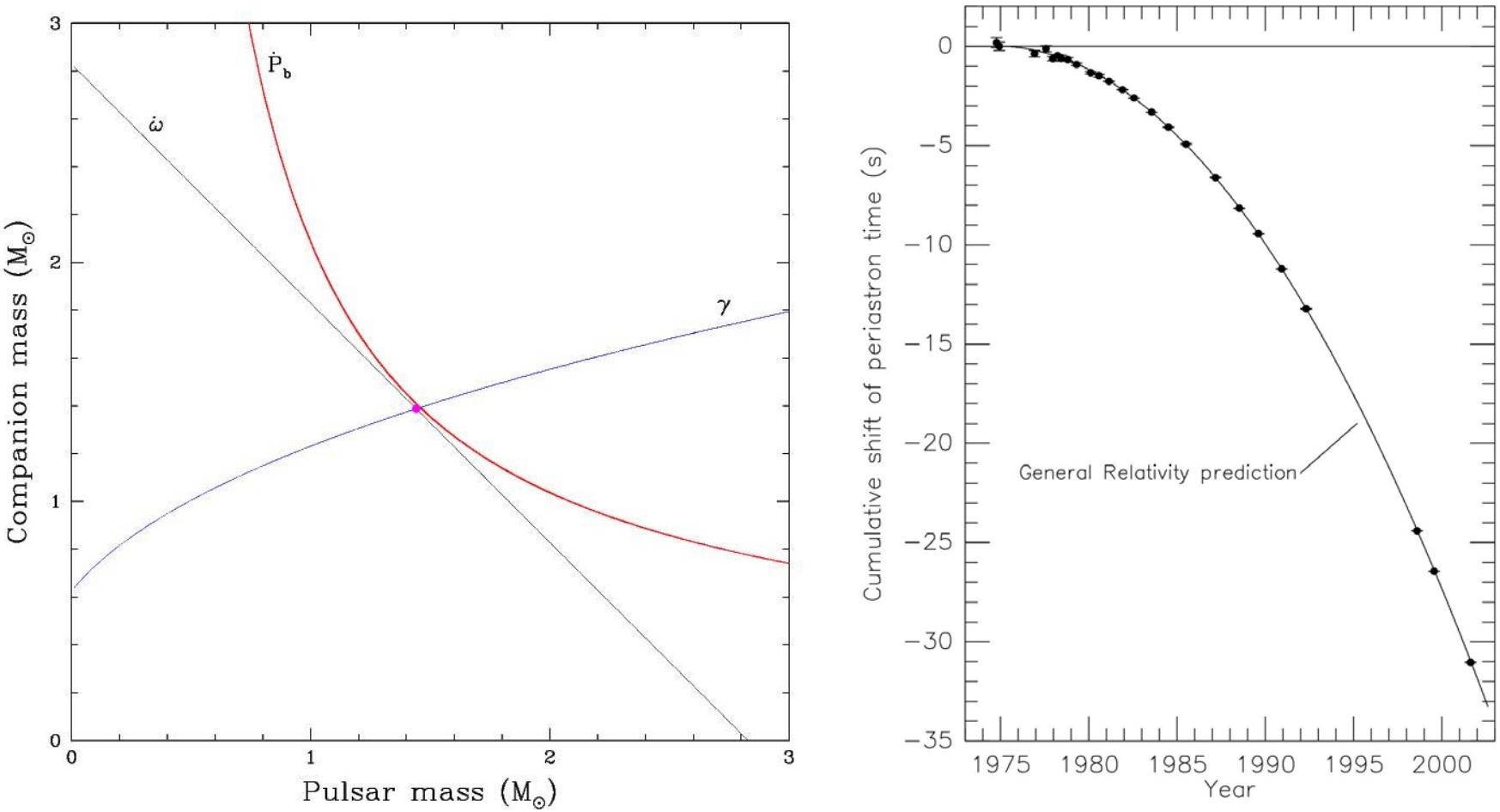

Figure 3. Timing results for the Hulse-Taylor binary pulsar B1913+16. The left panel shows the mass vs. mass plot for the pulsar and its companion neutron star. The three lines correspond to the three measured post-Keplerian parameters. The right panel shows the periastron shift caused by the decay of the orbit via emission of gravitational radiation. The detection of gravitational radiation resulted in a Nobel prize for Hulse and Taylor. (Figure provided by J. Weisberg).

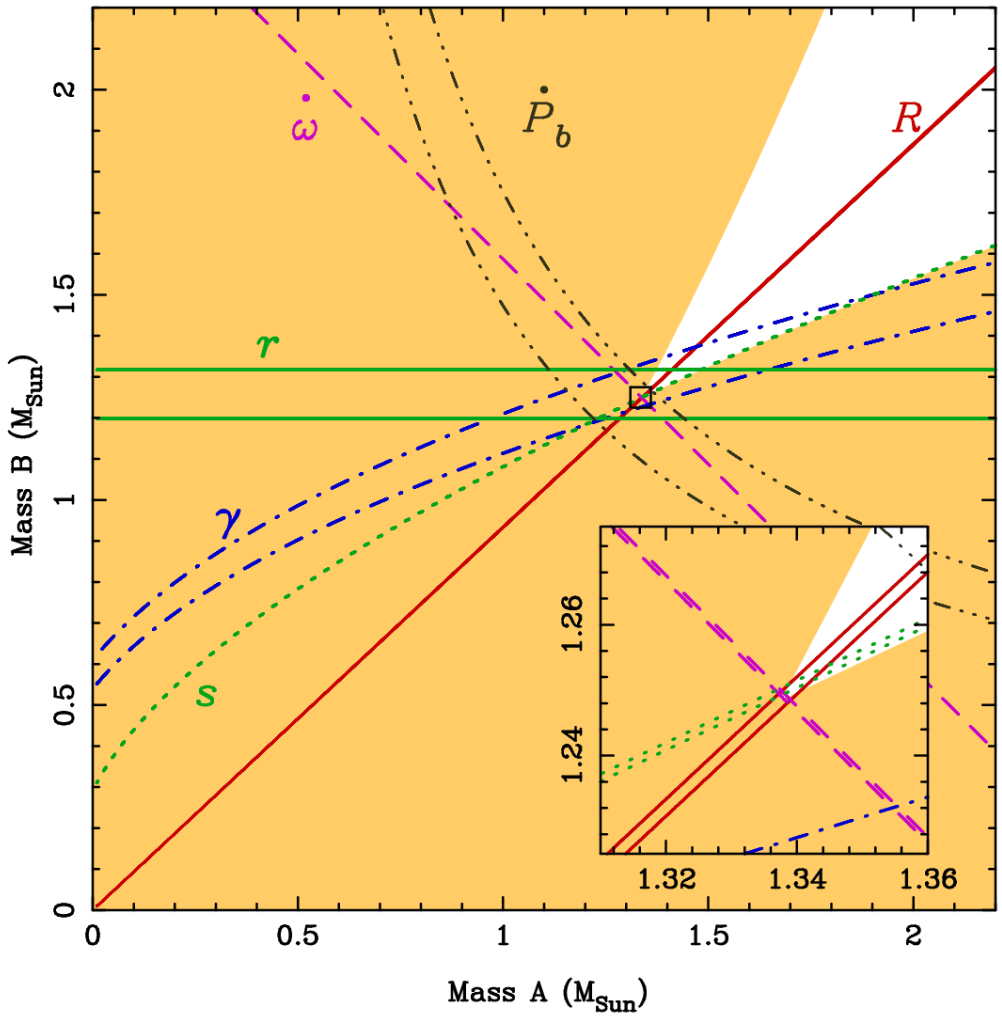

Figure 4: PSR J0737−3039 mass vs. mass diagram. As in Figure 3, the diagram shows lines corresponding to the post-Keplerian parameters measured for the system. In this case, though, six parameters were measured, including the mass ratio R since both neutron stars are pulsar clocks. These measurements have tested GR to ~0.05% (Kramer et al. 2006).

Sources

- Condon & Ransom
- "Pulsar Astronomy", Lyne & Graham-Smith
- "Handbook of Pulsar Astronomy", Lorimer & Kramer

http://www.astron.nl/astrowiki/doku.php?id=UvA_MSc_RadioAstronomy_2013

Questions?